

Upper critical fields and two-band superconductivity in $\text{Sr}_{1-x}\text{Eu}_x(\text{Fe}_{0.89}\text{Co}_{0.11})_2\text{As}_2$ ($x = 0.203$ and 0.463)

Rongwei Hu^{1,*}, Eun Deok Mun², M. M. Altarawneh^{2,†}, C. H. Mielke², V. S. Zapf², S. L. Bud'ko¹, P. C. Canfield¹

¹*Ames Laboratory, U.S. DOE and Department of Physics and Astronomy,
Iowa State University, Ames, IA 50011, USA and*

²*National High Magnetic Field Laboratory, Los Alamos National Laboratory, Los Alamos, New Mexico 87545, USA*
(Dated: June 15, 2018)

The upper critical fields, H_{c2} of single crystals of $\text{Sr}_{1-x}\text{Eu}_x(\text{Fe}_{0.89}\text{Co}_{0.11})_2\text{As}_2$ ($x = 0.203$ and 0.463) were determined by radio frequency penetration depth measurements in pulsed magnetic fields. H_{c2} approaches the Pauli limiting field but shows an upward curvature with an enhancement from the orbital limited field as inferred from Werthamer-Helfand-Hohenberg theory. We discuss the temperature dependence of the upper critical fields and the decreasing anisotropy using a two-band BCS model.

PACS numbers: 74.25.Dw, 74.25.Op, 74.70.Dd

The upper critical fields H_{c2} and its anisotropy are fundamental characteristics of a type-II superconductor, they provide information about the underlying electronic structure and can shed light on the mechanism of Copper pair breaking. Therefore for both understanding of superconductivity and potential application, extensive studies of H_{c2} have been performed on the recently discovered FeAs-based superconductors. Large upper critical fields have been observed for FeAs superconductors.¹⁻⁷ More interestingly, they exhibit pronounced upward curvature of H_{c2} , implying multi-band nature of these materials.^{5,8-10} In contrast to the high T_c cuprates with very large anisotropy, although they both possess a layered crystal structure, measurements of H_{c2} of the FeAs superconductors have revealed that the anisotropic ratio $\gamma = H_{c2}^{ab}/H_{c2}^c$ decreases with decreasing temperature and becomes nearly isotropic at low temperatures for the 122 and 111 type of FeAs materials.^{6-8,11}

Previous study of the Eu doped $\text{Sr}(\text{Fe}_{0.88}\text{Co}_{0.12})_2\text{As}_2$ demonstrated the interaction between the FeAs-based superconductivity and magnetism due to Eu^{2+} : in the disordered paramagnetic region of Eu^{2+} , superconductivity is weakly suppressed by spin-flip scattering off the local magnetic moments of Eu^{2+} ; it is further suppressed with developing long range antiferromagnetic order of Eu^{2+} and coexists with antiferromagnetism of Eu^{2+} as long as $T_c > T_N$.¹² It is of great interest to see how the superconductivity is modified by the magnetism of Eu^{2+} by mapping out the $H - T$ phase diagram.

Moreover, in the study of the interplay of superconductivity and magnetism, it is proposed by Jaccarino *et al*¹⁹ that for certain rare earth ferromagnetic metal, the external magnetic field, which in general inhibits superconductivity, may be cancelled by the effective exchange field H_{eff} of the magnetic moments, imposed on the conduction electrons, when H_{eff} is opposite to the direction of applied field. Therefore superconductivity can occur in two domains, one at low field, where pair-breaking field is still small, and one at high field in the compensation region. Experimentally, an anomalous en-

hancement of H_{c2} was first reported by Fischer *et al*¹³ in $\text{Sn}_{1.2(1-x)}\text{Eu}_x\text{Mo}_{6.35}\text{S}_8$ and $\text{Pb}_{1-x}\text{Eu}_x\text{Mo}_{6.35}\text{S}_8$ chevron phases and was suggested to be related to Jaccarino-Peter effect. A magnetic field induced superconductivity in the $H_{c2} - T$ phase diagram was indeed observed in $\text{Eu}_{0.75}\text{Sn}_{0.25}\text{Mo}_6\text{S}_{7.2}\text{Se}_{0.8}$ and fitted well with the Jaccarino-Peter scenario.¹⁴ Therefore, the properties of $\text{Sr}_{1-x}\text{Eu}_x(\text{Fe}_{0.89}\text{Co}_{0.11})_2\text{As}_2$, as possible candidates for observation of Jaccarino-Peter effect, are worth investigating.

In this paper we report the upper critical fields of $\text{Sr}_{1-x}\text{Eu}_x(\text{Fe}_{0.89}\text{Co}_{0.11})_2\text{As}_2$ ($x = 0.203$ and 0.463) single crystals determined by radio frequency contactless penetration depth measurements. The two selected samples are the representative concentrations in the disordered paramagnetic region and coexistence region of superconductivity and antiferromagnetism. We find that for both concentrations the curves of $H_{c2}(T)$ can be consistently explained by the two-band model and the anisotropy decreases with temperature approaching an isotropic state at low temperatures.

Single crystals of $\text{Sr}_{1-x}\text{Eu}_x(\text{Fe}_{0.89}\text{Co}_{0.11})_2\text{As}_2$ were grown from self flux, as describe in Ref. 12. Chemical composition was determined by wavelength dispersive x-ray spectroscopy (WDS) in a JEOL JXA-8200 electron microscope. Magnetic susceptibility was measured in a Quantum Design MPMS. The temperature and magnetic field dependences of the electrical resistance were measured using the four probe ac ($f = 16\text{Hz}$) technique in a Quantum Design PPMS. Radio frequency (rf) contactless penetration depth measurements were performed on the single-crystal sample in a 60 T pulsed field magnet with a 10 ms rise time and a 40 ms extended decay. The rf technique is highly sensitive to small changes ($\sim 1-5$ nm) in the rf penetration depth, thus it is an accurate method for determining the upper critical field in anisotropic superconductors.¹⁵ Small single crystals were selected because of the eddy current heating in pulsed field. To determine the upper critical-field anisotropy, the single crystal was measured in two $H \parallel ab$ and $H \parallel c$ configurations. More details about this technique can be

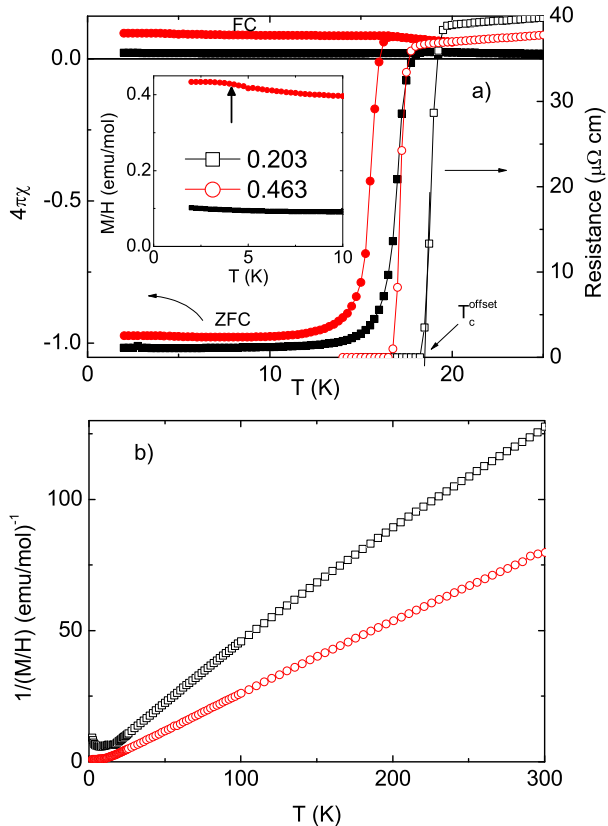


FIG. 1: a) Low temperature magnetic susceptibility measured in a magnetic field 100 Oe applied in ab plane and resistivity in zero field. Inset shows an zoom-in view of the field-cooled curve, arrow indicates the antiferromagnetic transition. b) Inverse in-plane magnetic susceptibility measured in 10 kOe.

found in Ref.4, 17, 18.

The actual compositions of the two samples determined by WDS were $\text{Sr}_{0.797}\text{Eu}_{0.203}(\text{Fe}_{0.888}\text{Co}_{0.112})_2\text{As}_2$ and $\text{Sr}_{0.537}\text{Eu}_{0.463}(\text{Fe}_{0.885}\text{Co}_{0.115})_2\text{As}_2$. For brevity, we denote them as Eu20 and Eu46 sample in the following text. The Co concentrations are consistent with the optimal doping, $x \sim 0.12$, for $\text{Sr}(\text{Fe}_{1-x}\text{Co}_x)_2\text{As}_2$ as in Ref. 12. Figure 1(a) shows the low temperature magnetic susceptibility and resistivity of the two samples. The large diamagnetic shielding indicates bulk superconductivity. The superconducting transition temperatures inferred from the first deviation point from the normal magnetic susceptibility of the zero-field-cool curve are 18 K and 16.2 K for Eu20 and Eu46 respectively. The Eu46 sample shows a weak anomaly due to antiferromagnetic ordering of Eu^{2+} at 3.5 K as indicated in the inset of Fig. 1(a). The T_c in resistivity as inferred from by extrapolating the steepest slope to zero resistance are 18.3 K and 16.8 K for the two samples, in agreement with the magnetic susceptibility measurements. The inverse

in-plane magnetic susceptibility measured in 10 kOe of the two samples is plotted in Fig.1 (b). The Curie-Weiss fits above 150 K give an estimated Eu concentration of 0.215 and 0.469 by assuming $7.94 \mu_B/\text{Eu}^{2+}$ ion. Thus all the above observations are consistent with those in Ref. 12 and show that Eu20 is in the disordered paramagnetic region of Eu^{2+} and Eu46 is in the coexistence region of superconductivity and antiferromagnetism.

The frequency shift as a function of magnetic field applied parallel and perpendicular to the ab plane at different temperatures from 1.5 to 19 K for Eu20 is shown in Fig. 2. The normal state has a smooth and nearly linear field dependence as manifested by the 19 K curve.¹⁶ H_{c2} is identified as the point at which the slope of the ΔF intercepts the normal state background of 19 K. Other criterion, e.g. first point deviating from the normal state background can be used and the difference between these two criteria is taken as the error bar for H_{c2} . For $H \parallel c$ in Fig. 2(b), the sample has a weaker coupling to the detection coil, resulting in a smaller but still easily resolvable frequency shift. The same rf measurements were performed on Eu46 sample for both orientations for temperatures down to 0.51 K and shown in Fig. 3. In the previous study in Ref. 12, it has been shown that the Eu^{2+} moments undergo a metamagnetic transition from antiferromagnetic to ferromagnetic above a magnetic field of 4 kOe. Thus it behaves as a superconductor with ferromagnetically coupled Eu^{2+} moments at low temperature high field. In order to look for possible Jaccarino-Peter effect, the frequency shift of Eu46 sample was measured in field up to 60 T at the base temperature 0.51 K for both directions (inset in Fig. 3(b)). No anomaly associated with superconductivity can be observed in high fields. So either the magnetic field is still too low to compensate the exchange field or the exchange field has the same sign as the external field then no cancellation can be realized.

Figure 4 shows the $H_{c2}(T)$ curves for $H \parallel ab$ (H_{c2}^{ab}) and $H \parallel c$ (H_{c2}^c) of both samples. For the Eu20 sample, H_{c2}^{ab} is almost linear close to T_c , a traditional Werthamer-Helfand-Hohenberg (WHH) behavior, but H_{c2}^c exhibits a significant upward curvature. This negative curvature is even more pronounced for the Eu46 sample in Fig. 4(b) for both field orientations. The dashed lines in Fig. 4 are fits to the conventional one-band WHH theory.²⁰ The H_{c2} values from direct measurements are far above the prediction of WHH theory, except for the $H \parallel ab$ curve of Eu20 sample (see later discussion). The other mechanism for limiting H_{c2} is the Pauli spin paramagnetic effect as a result of Zeeman effect exceeding the condensation energy of Cooper pairs, given by $\mu_0 H_p = 1.84T_c$ for isotropic s-wave pairing.²¹ $\mu_0 H_p$ is estimated to be 30.9 T and 29.4 T for Eu20 and Eu46 respectively. These values are close to the experimental results extrapolated to 0 K, implying that the Pauli paramagnetic effect might be the dominant pair breaking mechanism for limiting the upper critical fields in these compounds.

On the other hand, the anomalous upward curva-

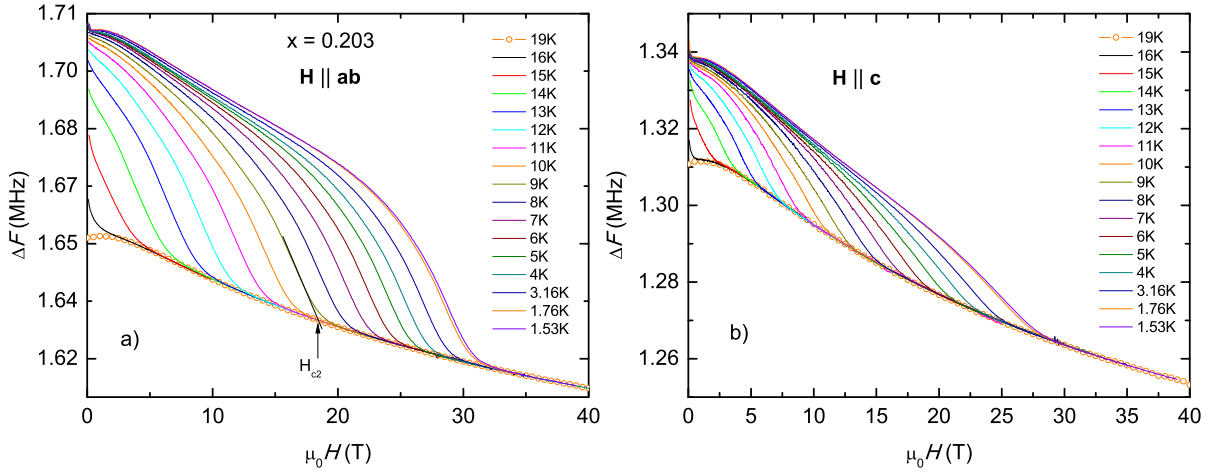


FIG. 2: Frequency shift (ΔF) as a function of magnetic field for $H \parallel ab$ and $H \parallel c$ for Eu20 sample at selected temperatures. Open symbols are ΔF taken at 19 K as a normal state, background signal. It shows the criterion to determine H_{c2} .

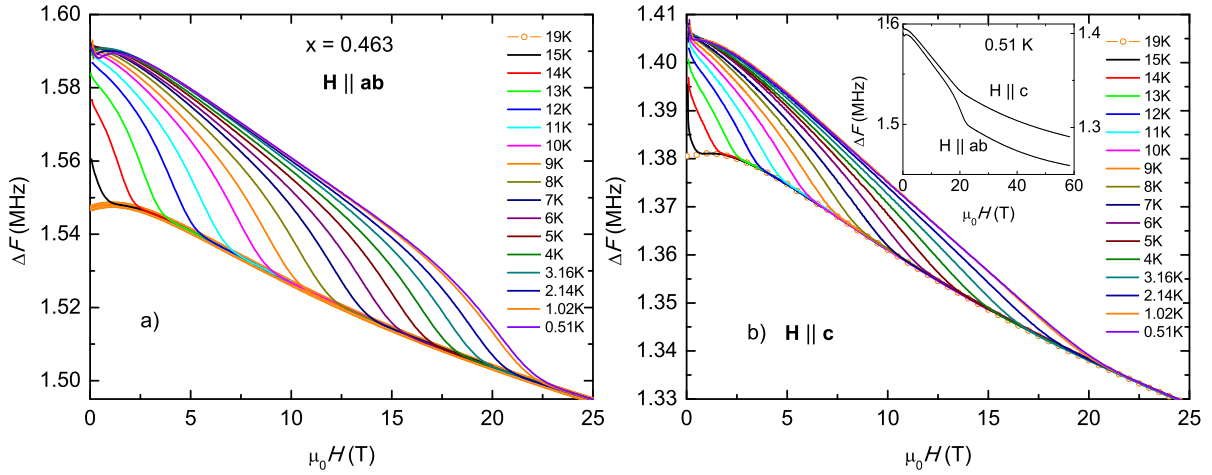


FIG. 3: ΔF as a function of magnetic field for $H \parallel ab$ and $H \parallel c$ for Eu46. Inset in (b) shows the measurements up to 60 T at the base temperature of 0.51 K.

ture of $H_{c2}(T)$ has been observed in other multiband systems like MgB_2 ²² and recently in FeAs superconductors e.g. $\text{Ba}(\text{Fe}_{0.9}\text{Co}_{0.1})_2\text{As}_2$ ⁵, $\text{LaFeAsO}_{0.89}\text{F}_{0.11}$ ⁸, $\text{NdFeAsO}_{0.7}\text{F}_{0.3}$ ⁹ and $\text{Sr}(\text{Fe}_{0.9}\text{Co}_{0.1})_2\text{As}_2$ thin film¹⁰ and explained within a two-band BCS model by taking into account the inter and intra band scattering in H_{c2} .²² In the two-band s-wave theory, the intra and interband interaction is described by a 2×2 matrix of the BCS coupling constants λ_{mn} , for which λ_{11} and λ_{22} quantify the intraband coupling and λ_{12} and λ_{21} describe interband

coupling. H_{c2} is described by a parametric equation²²

$$\ln \frac{T}{T_{c0}} = -\left(U(h) + U\left(\frac{D_2}{D_1}h\right) + \frac{\lambda_0}{w} \right) / 2 + \left[\left(U(h) - U\left(\frac{D_2}{D_1}h\right) - \frac{\lambda_-}{w} \right)^2 / 4 + \frac{\lambda_{12}\lambda_{21}}{w} \right]^{1/2}$$

$$U(h) = \psi(1/2 + h) - \psi(1/2)$$

$$H_{c2} = 2\phi_0 k_B T h / \hbar D_1$$

where $\psi(x)$ is the digamma function, ϕ_0 is the flux quantum, k_B is the Boltzmann constant, \hbar is the plank constant, $D_{1,2}$ are the anisotropic diffusivities of each band, for H_{c2}^{ab} the diffusivity D_1 should be replaced by $(D_1^{ab} D_1^c)^{1/2}$, $\lambda_- = \lambda_{11} - \lambda_{22}$, $\lambda_0 = (\lambda_-^2 + 4\lambda_{12}\lambda_{21})^{1/2}$, $w = \lambda_{11}\lambda_{22} - \lambda_{12}\lambda_{21}$. Since only the product of λ_{12} and λ_{21} appears in the equation, we can assume $\lambda_{12} = \lambda_{21}$.

TABLE I: Parameters of the fits to the two-band model for $\text{Sr}_x\text{Eu}_x(\text{Fe}_{0.89}\text{Co}_{0.11})_2\text{As}_2$

x	$\langle \begin{smallmatrix} D_1^{ab} & D_1^c \\ D_2^{ab} & D_2^c \end{smallmatrix} \rangle$ (cm^2/s)	$\langle \begin{smallmatrix} \lambda_{11} & \lambda_{12} \\ \lambda_{21} & \lambda_{22} \end{smallmatrix} \rangle$	$\mu_0 H_{c2}^{ab}(0)$ (T)	$\mu_0 H_{c2}^c(0)$ (T)	$\xi^{ab}(0)$ (nm)	$\xi^c(0)$ (nm)
0.203	$\langle \begin{smallmatrix} 0.16 & 1.35 \\ 0.36 & 0.15 \end{smallmatrix} \rangle$	$\langle \begin{smallmatrix} 0.19 & 0.194 \\ 0.194 & 0.21 \end{smallmatrix} \rangle$	31.6	30.4	3.3	3.2
0.463	$\langle \begin{smallmatrix} 0.79 & 2.27 \\ 0.28 & 0.25 \end{smallmatrix} \rangle$	$\langle \begin{smallmatrix} 0.2 & 0.082 \\ 0.082 & 0.2 \end{smallmatrix} \rangle$	22.4	20.4	4.0	3.7

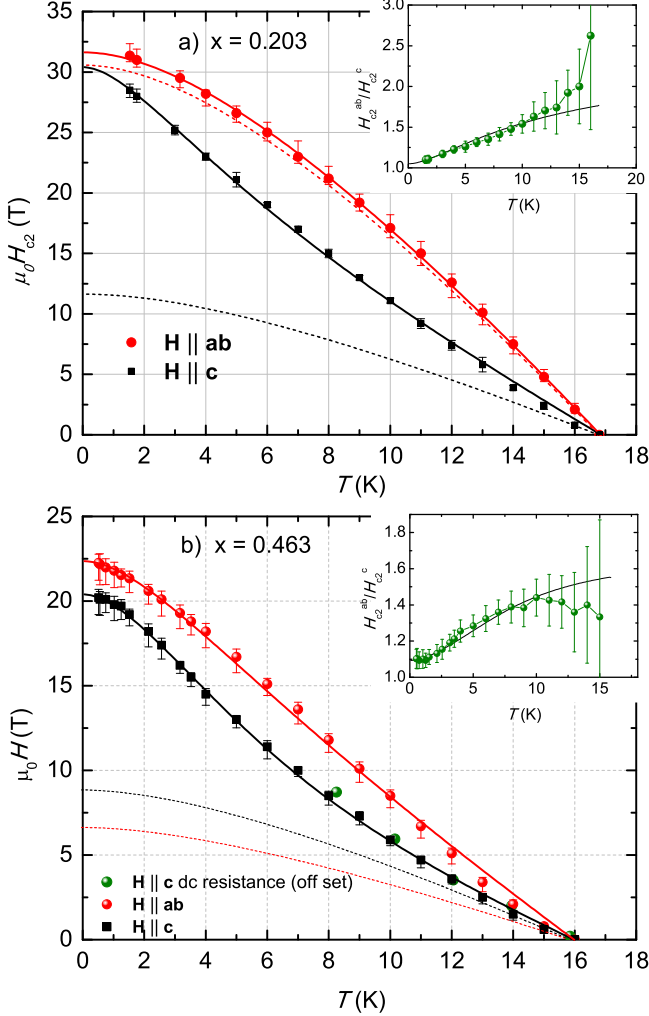


FIG. 4: Anisotropic $H_{c2}(T)$ for Eu20 and Eu46 single crystals. The green circles in (b) are obtained from the resistivity measurement, in excellent agreement with the pulsed field rf shift measurement. The dotted lines are fits to WHH formula. The solid lines are fits to the two-band model. Insets show the temperature dependence of the anisotropy $\gamma = H_{c2}^{ab}/H_{c2}^c$ and the solid lines are the calculated curve of the two-band model fits.

The fits to both H_{c2}^{ab} and H_{c2}^c for each sample are performed simultaneously in a self-consistent manner. The model fits the data remarkably well, it captures the main features of the H_{c2} curves. The fitting parameters are listed in Table I. In terms of diffusivity, the two bands exhibit strong asymmetry, i.e. the diffusivity ratio $\sqrt{D_2^{ab}D_2^c}/\sqrt{D_1^{ab}D_1^c} \sim 0.5$ and 0.2 for Eu20 and Eu46 respectively. Thus superconductivity results from an anisotropic band with high diffusivity and a more isotropic band with smaller diffusivity. It should be noted that for the Eu20 sample H_{c2}^c shows negative curvature whereas H_{c2}^{ab} shows behavior similar to that conforms with the conventional WHH theory. The two types of curvature for different field orientations have also been observed in $\text{Ba}(\text{Fe}_{0.93}\text{Co}_{0.07})_2\text{As}_2$.²³ But here we are describing both of them within the two-band model. For equal diffusivities of the two bands, i.e. $\eta = D_2/D_1 = 1$, the parametric equation of above reduces to the one-gap de-Gennes-Maki formula in WHH theory, $\ln t + U(h) = 0$.²² The diffusivity ratio of the Eu20 sample, $\eta^{ab} = D_2^{ab}/(D_1^{ab}D_1^c)^{1/2}$ and $\eta^c = D_2^c/D_1^c$, is 0.77 and 0.11 for $H \parallel ab$ and $H \parallel c$ respectively. Therefore it is reasonable to expect H_{c2}^{ab} with near unity η to show WHH-like behavior in contrast to H_{c2}^c with much lower η to be two-band-like.

The Eu20 sample shows strong interband pairing, i.e. $\lambda_{12}\lambda_{21} \simeq \lambda_{11}\lambda_{22}$, whereas the two bands become more non-interacting in the Eu46 sample, as indicated by $\lambda_{12}\lambda_{21} \ll \lambda_{11}\lambda_{22}$. It is noteworthy that the intraband pairing strength, λ_{11} and λ_{22} , remains almost unchanged for Eu concentration increases from 0.203 to 0.463, only the interband coupling decreases, with T_c decreases slowly from 16.8 K to 16 K. This observation may imply that superconductivity could be dominated by the intraband pairing and not particularly sensitive to disorder and interband scattering. With the fitted values of H_{c2} at 0 K, we can estimate the anisotropic coherence length using $\xi^{ab} = \sqrt{\phi_0/2\pi H_{c2}^c}$ and $\xi^c = \phi_0/2\pi \xi^{ab} H_{c2}^{ab}$ (Table I). Both ξ^{ab} and ξ^c are much larger than the spacing between the superconducting FeAs layers ($\sim 6\text{\AA}$) in $\text{Sr}_{1-x}\text{Eu}_x(\text{Fe}_{0.89}\text{Co}_{0.11})_2\text{As}_2$, suggesting a 3D characteristic of superconductivity.

The anisotropy of H_{c2} is plotted in the insets of Fig. 4. Both γ decrease with decreasing temperature and approach 1 at zero temperature. It is qualitatively similar to that of the LiFeAs ,⁶ $(\text{Ba,K})\text{Fe}_2\text{As}_2$,^{4,11} and $\text{LaFeAsO}_{0.89}\text{F}_{0.11}$.⁸ The isotropy of H_{c2} in FeAs super-

conductors with different carrier dopings is unexpected since distinctive hole and electron Fermi surfaces may be responsible for superconductivity with different dopings. For our Eu20 and Eu46 samples, there could be two factors contributing to the decreasing anisotropy: i) at low temperature, band 2 with lower band anisotropy $D_2^{ab}/D_2^c \sim 2.4 - 1.1$ may become more important than band 1 with $D_1^{ab}/D_1^c \sim 0.12 - 0.35$; ii) the two bands have opposing anisotropy of diffusivity, for band 1, $(D_1^{ab}/D_1^c) < 1$, whereas for band 2, $(D_2^{ab}/D_2^c) > 1$. The calculated γ from the fits are shown as the solid lines in the insets. They well reproduce the temperature dependence of γ within error bars.

To summarize, we measured the anisotropic $H_{c2}(T)$ for single crystals of $\text{Sr}_{1-x}\text{Eu}_x(\text{Fe}_{0.89}\text{Co}_{0.11})_2\text{As}_2$ ($x = 0.203$ and 0.463). Despite the presence of Eu^{2+} moment, the Jaccarino-Peter effect is not observed up to 60 T at base temperature of 0.5 K, it may be intrinsically absent in this system or higher field is needed. H_{c2} deviates from the WHH behavior as manifested by the upward curva-

ture and is probably limited by the Pauli paramagnetic pair breaking. The temperature dependence of H_{c2} is well described by a model of two bands with opposing anisotropy and large diffusivity difference. The H_{c2} becomes more isotropic at low temperature.

This work was carried out at the Iowa State University and supported by the AFOSR-MURI grant #FA9550-09-1-0603 (R. H. and P. C. C.). Part of this work was performed at Ames Laboratory, US DOE, under contract # DE-AC02-07CH 11358 (S. L. B. and P. C. C.). S. L. B. was also partially supported by the State of Iowa through the Iowa State University. Work at the NHMFL is supported by the NSF, the DOE and the State of Florida.

*Present address: Center for Nanophysics & Advanced Materials and Department of Physics, University of Maryland, College Park MD 20742-4111, USA.

†Present address: Department of physics, Mu'tah University, Mu'tah, Karak, 61710, Jordan.

-
- ¹ M. Shahbazi, X. L. Wang, C. Shekhar, O. N. Srivastava, Z. W. Lin, J. G. Zhu, and S. X. Dou
- ² C. Senatore, R. Flukiger, M. Cantoni, G. Wu, R. H. Liu, and X. H. Chen, *Phys. Rev. B* **78**, 054514 (2008)
- ³ Xiaolin Wang, Shaban Reza Ghorbani, Germanas Peleckis, Shixue Dou, *Adv. Mater.* **21**, 236 (2009)
- ⁴ M. M. Altarawneh, K. Collar, and C. H. Mielke, N. Ni, S. L. Bud'ko, and P. C. Canfield, *Phys. Rev. B* **78**, 220505(R) (2008)
- ⁵ Mika Kano, Yoshimitsu Kohama, David Graf, Fedor Balakirev, Athena S. Sefat, Michael A. McGuire, Brian C. Sales, David Mandrus, and Stanley W. Tozer, *J. Phys. Soc. Jpn.* **78**, 084719 (2009)
- ⁶ J. L. Zhang, L. Jiao, F. F. Balakirev, X. C. Wang, C. Q. Jin, H. Q. Yuan, *Phys. Rev. B* **83**, 174506 (2011)
- ⁷ N. Ni, S. L. Bud'ko, A. Kreyssig, S. Nandi, G. E. Rustan, A. I. Goldman, S. Gupta, J. D. Corbett, A. Kracher, and P. C. Canfield, *Phys. Rev. B* **78**, 014507 (2008)
- ⁸ F. Hunte, J. Jaroszynski, A. Gurevich, D. C. Larbalestier, R. Jin, A. S. Sefat, M. A. McGuire, B. C. Sales, D. K. Christen & D. Mandrus, *Nature* **453**, 903 (2008)
- ⁹ J. Jaroszynski, F. Hunte, L. Balicas, Youn-jung Jo, I. Raicevic, A. Gurevich, D. C. Larbalestier, F. F. Balakirev, L. Fang, P. Cheng, Y. Jia, and H. H. Wen, *Phys. Rev. B*, **78**, 174523 (2008)
- ¹⁰ S. A. Baily, Y. Kohama, H. Hiramatsu, B. Maiorov, F. F. Balakirev, M. Hirano, and H. Hosono, *Phys. Rev. Lett.* **102**, 117004 (2009)
- ¹¹ H. Q. Yuan, J. Singleton, F. F. Balakirev, S. A. Baily, G. F. Chen, J. L. Luo, and N. L. Wang, *Nature* **457**, 565 (2009)
- ¹² Rongwei Hu, Sergey L. Bud'ko, Warren E. Straszheim, Paul C. Canfield, *Phys. Rev. B* **83**, 094520 (2011)
- ¹³ Ø Fischer, M. Decroux, S. Roth, R. Chevrel and M Sergeant, *J. Phys. C: Solid State Phys.*, **8**, 474 (1975)
- ¹⁴ H. W. Meul, C. Rossel, M. Decroux, and Ø Fischer, G. Remenyi, A. Briggs, *Phys. Rev. Lett.* **53**, 497-500 (1984)
- ¹⁵ C. Mielke, J. Singleton, M.-S. Nam, N. Harrison, C. C. Agosta, B. Fravel, and L. K. Montgomery, *J. Phys.: Condens. Matter* **13**, 8325 (2001)
- ¹⁶ E. D. Mun, M. M. Altarawneh, C. H. Mielke, and V. S. Zapf, R. Hu, S. L. Bud'ko, and P. C. Canfield, *Phys. Rev. B* **83**, 100514(R) (2011)
- ¹⁷ T. Coffey, Z. Bayindir, J. F. DeCarolis, M. Bennett, G. Esper, and C. C. Agosta, *Rev. Sci. Instrum.* **71**, 4600 (2000)
- ¹⁸ M. M. Altarawneh, C. H. Mielke, and J. S. Brooks, *Rev. Sci. Instrum.* **80**, 066104 (2009)
- ¹⁹ V. Jaccarino and M. Peter, *Phys. Rev. Lett.* **9**, 290 (1962)
- ²⁰ N. R. Werthamer, E. Helfand, P. C. Hohenberg, *Phys. Rev.* **147**, 295 (1966)
- ²¹ A. M. Clogston, *Phys. Rev. Lett.* **9**, 266 (1962)
- ²² A. Gurevich, *Phys. Rev. B* **67**, 184515 (2003)
- ²³ V. A. Gasparov, L. Drigo, A. Audouard, D. L. Sun, C. T. Lin, S. L. Bud'ko, P. C. Canfield, F. Wolff-Fabris and J. Wosnitza, *JETP Letters*, **93**, 667 (2011)